GLOBAL-LOCAL ANALYSIS OF BONDED SKIN-TO-STIFFENER JOINTS IN POST-BUCKLED PANELS

P. Coudor [◇⋆] , S. Van der Veen [◁] , A. Beakou [◇]

[◇] Laboratoire de Mécanique et Ingénieries (LaMI), Institut Français de Mécanique Avancée (IFMA), Université Clermont II, Campus des Cézeaux, BP 265, 63175 Aubière cedex, France
[◁] Development Engineer in charge of Structures Analysis for Alcan Aerospace, BP 42, 63502 Issoire cedex, France [⋆⋆]

[⋆] Corresponding author: pcoudor@ifma.fr
[⋆⋆] New affiliation: Airbus France, Metallic Materials Processes

Keywords: *bonded joints, stiffened panels, post-buckling*

Abstract

Recent advances in aeronautics and material science allow for a significant increase in load capacity; consequently, structural parts are more stressed than in the past. In most cases, stresses and strains cannot be determined accurately enough using conventional closed form engineering formulae. Therefore, even if much more time-consuming, finite element analysis is used. Because of a high ratio between panel length and adhesive thickness, models need a large number of elements. Thus, computing time can be very long. The aim of this paper is to present a global-local approach to reduce this time. First, a global shell elements model is developed. Second, a local solid elements model is generated from the displacement obtained in the global model. Finally, global-local FEA enables greater precision.

1 Introduction

Today's high-strength and damage-tolerant materials allow for significant increases in load capacity and stress limits in aircraft structures. In stiffened panels - the basic building blocks of these structures - joints between skin and stiffeners will need to transfer more load. Adhesive bonding of stiffeners to skins has several advantages over other joining techniques: no fatigue, potentially better crack bridging in the presence of serious damage and in many cases improved buckling stability. But for heavily loaded components, the strength of bonded joints is often in question. The present work is concerned with the stress analysis of adhesively bonded skin-to-stiffener joints in post-buckling. To this end, a fully non-linear finite element global-local approach was used. First, a global shell model was analysed and validated against an experiment described in the literature. Second, a local model of the attached flange, the adhesive layer and part of the skin was developed, using solid elements. The strains and stresses resolved from the local model were validated against those observed in the global model and subsequently served to predict failure of the adhesive or the adherents, using simple strain- and stress- based failure criteria from the literature. This global-local approach could be used to analyse the strength and damage tolerance of adhesively bonded panels in post-buckling (partial debonding) and to simulate progressive damage and debonding using more advanced models of damage to the adhesive.

2 Global finite element modelling approach

The global finite element model is based on the paper of Murphy and al. [1]. It provides recent computed and experimental results on welded stiffened panels. These results will be used in the present paper to validate the global model. It consists of a single stiffener cripping specimen design, with a Z-section longitudinal stiffener (7075-T76511) and a flat skin base (2024-T3). The geometric details are given in figure 1.

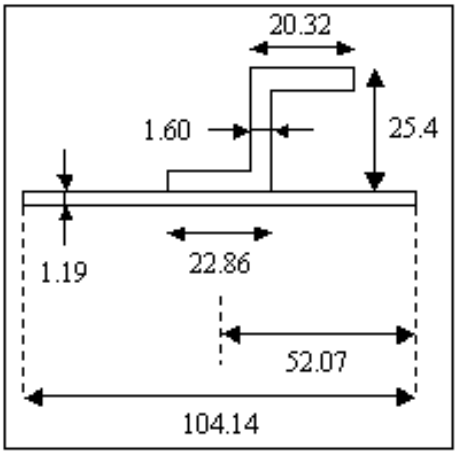

Fig. 1 Principle geometric details in millimeters

Panel length is equal to 165.1 mm and adhesive thickness to 0.2 mm. Murphy and al. model a welded joint with a skin pad-up under the stiffener area. In this paper, to simplify modelling, the pad-up is not represented. The stiffener is bonded to the skin. Therefore, the stiffened panel used in this paper is more flexible. Shell elements are used to model skin and stiffener. The material properties of the skin and stiffener are shown in figure 2. Adhesive modelling is described in the folowing section.

2.1 Modelling of bonded joints in the global model

2.1.1 Element types

As Murphy and al. did in [1], Scott and al. tied skin nodes to the corresponding flange nodes with all six degrees of freedom being constrained

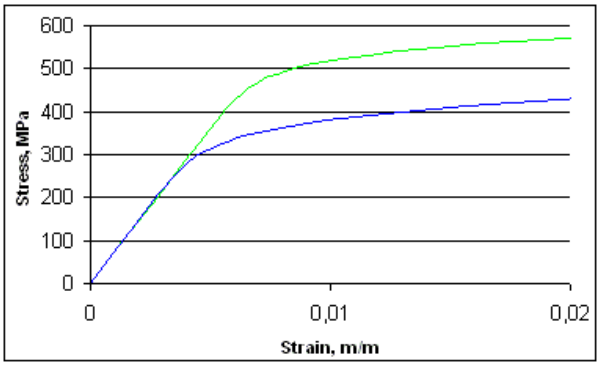

Fig. 2 Stress-strain graph obtained from Ramberg-Osgood parameters

with rigid bar elements [2] or with rigid links elements [1]. In this paper, for an initial approach, the adhesive is modelled by beam elements. Beams were found more computationally efficient than the recently implemented RBE2s (MSC.Marc 2005), which deal effectively with rigid body rotations, while giving identical results (Figure 3).

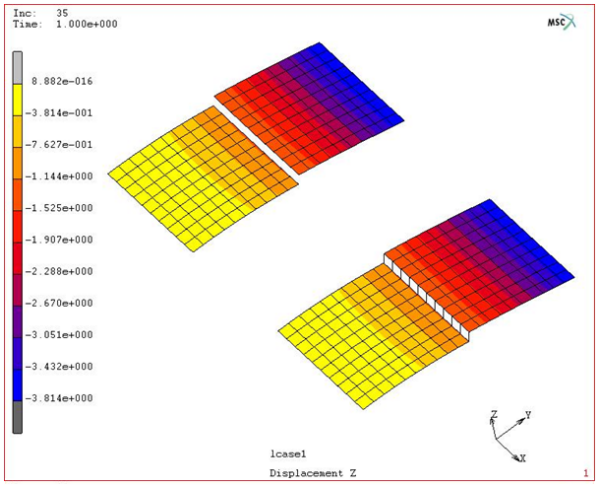

Fig. 3 Identical out-of-plane displacement after large displacement analysis of two 10 mm x 10 mm x 0.5 mm plates joined with a 1 mm offset, using RBE2s (top) or beams (bottom) [3]

2.1.2 Material properties

Properties for FM73 were deduced from shear data found in the literature [4] [5]. Properties are obtained at room temperature (Figure 4). First principles were used to derive tensile stress-strain

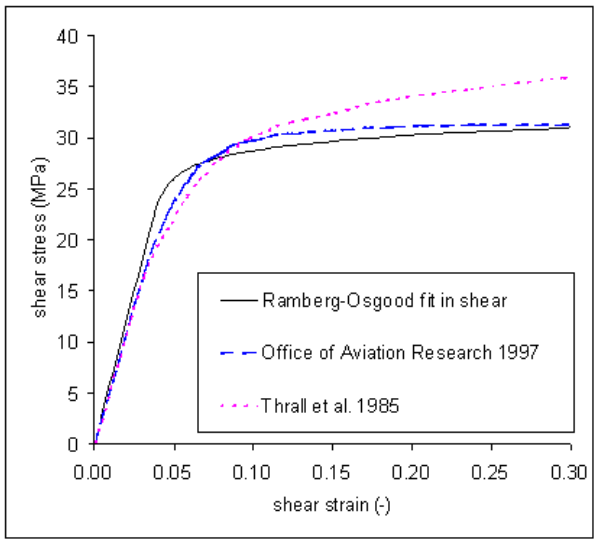

Fig. 4 Shear stress-strain data from literature and fitted; conservative Ramberg-Osgood curve

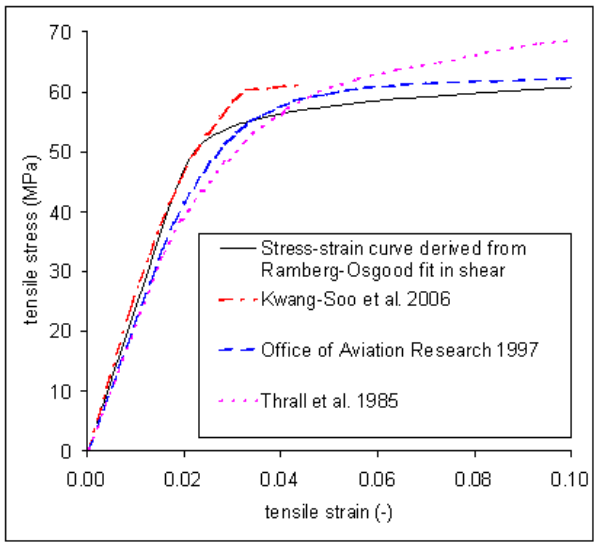

Fig. 5 Tensile stress-strain derived from shear data and verification curve from literature

data from the fitted shear curve:

$$\varepsilon = \cos\frac{\gamma}{2} + \sin\frac{\gamma}{2} - 1 \tag{1}$$

$$\sigma = 2\tau \tag{2}$$

$$E = 2G(1+\nu) \tag{3}$$

where ε is tensile strain, γ shear strain, σ tensile stress; τ shear stress, E Young's modulus, G shear modulus and ν Poisson's ratio (taken as 0.25). The result was verified against a stress-strain curve found in another publication [6] (Figure 5).

2.2 Boundary conditions

For the global model, boundary conditions were chosen so as to simulate an embedded panel, similar to boundary conditions reported in [1]. The edge at $z = 0$ mm is embedded and for the edge at $z = 165.1$ mm the degrees of freedom are constrained except for translation along the z-axis. Link elements are used to centralize reaction forces on one node. This node is connected with all the nodes of the edge $z = 165.1$ mm. A displacement along the z-axis equal to -2 mm is applied to this node.

2.3 Solution strategy

The global model corresponds to the first step of a global-local analysis. The aim of this study is to obtain global results and a post file containing these results. For the post-buckling analysis, the mesh was perturbed at the first increment using the first eigenmode, with the deformation amplitude at 1/1000 of the bay length between the frames or ribs. Geometric non-linearity was activated but the large strain capability was left deactivated, because only very small plastic deformation was expected. The solution was achieved with the arc length method, using the MARC 2005 solver [7] [8].

2.4 Results

Figure 6 presents the deformed shape with displacement along the y-axis. From this study, end-shortening versus compression load curves can be plotted. Figure 7 shows curves obtained by Murphy and al. [1] and that obtained with the FEA global model. These curves show that the global model is, as previously supposed, more flexible than the Murphy and al. model. These results are coherent and critical load is equal to 60 kN. This model can then be used to introduce displacement into the local model.

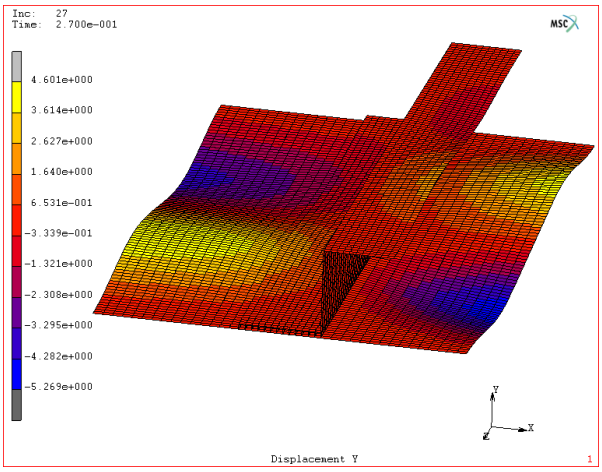

Fig. 6 Deformed shape with displacement along the y-axis for the global model

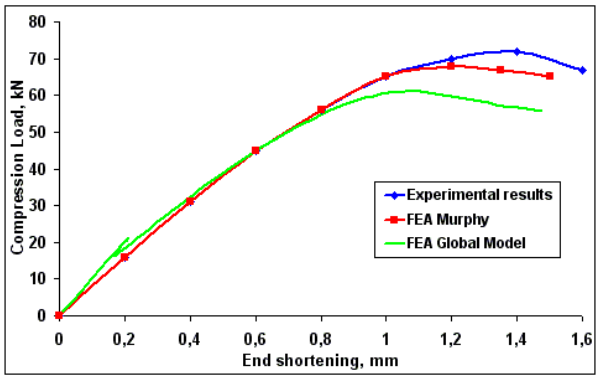

Fig. 7 End-shortening versus compression load curves given by [1] and global FEA

3 Local stiffener-to-skin joint models

3.1 Element types

8-node brick elements are used to mesh the local model. Refinement is done near the adhesive area to be more accurate (Figure 8). Figure 9 presents the relative positions of the local and the global models. In order to reduce computing time, 4 small local models are computed along the z-axis. As shown in figure 10, 3 local models are added to prevent edge effects. Then with a simple matlab routine which selects only parts far enough from the edges, the results are deduced all along the z-axis.

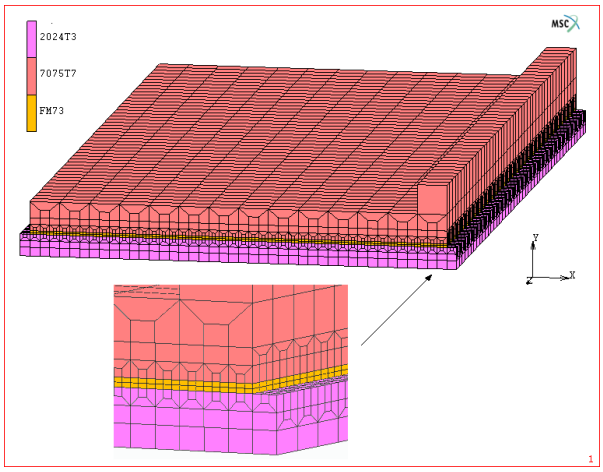

Fig. 8 Local model meshing

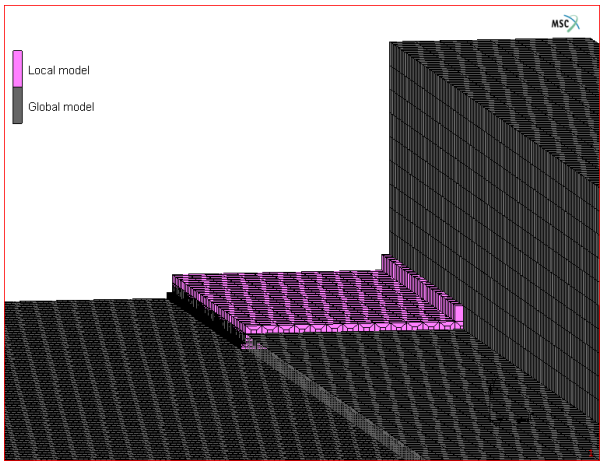

Fig. 9 Relative positions of the local and the global models

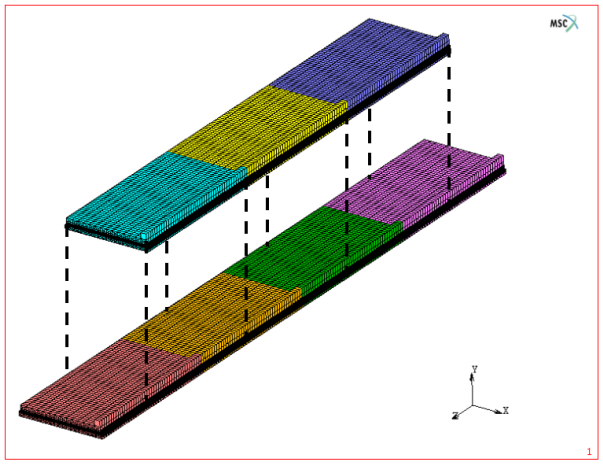

Fig. 10 All the local models used to obtain the results

3.2 Boundary conditions

The local model is the second step in the global-local analysis. Kinematic boundary conditions are introduced to the edges from the post file containing the global results [9] [10].

3.3 Solution strategy

Local models are computed as static non-linear models. Computation substeps correspond to the increments of the global model. Computation is stopped at the step corresponding to the failure of the global model.

3.4 Joint failure criteria for bonded panels

Figure 11 shows the failure modes in adhesively bonded joints identified by Heslehurst and Hart-Smith [11]. In this paper, only adhesive failure modes are considered.

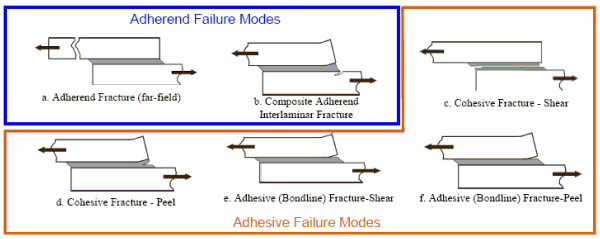

Fig. 11 Failure modes in adhesively bonded joints identified by Heslehurst and Hart-Smith [12] [11]

Adhesives are more susceptible to failure due to tensile strain than pure shear and compression. In some cases, nonlinear behaviour dominates and failure strain can exceed 100% [11]. Thus, for the cohesive failure of ductile adhesives, the maximum strain criterion is usually applied. It is given as

$$\frac{\varepsilon_{eqv}}{S_{eqv}} = 1 \tag{4}$$

where ε_{eqv} is the von Mises equivalent strain and S_{eqv} is the failure strain [11] [13].
Failure of the spew fillet is another case to be considered for adhesive failure. It is caused by tensile stress [11]. The maximum principal stress criterion is applied. It is given as

$$\frac{\sigma_p^{\max}}{X_T} = 1 \tag{5}$$

where $\sigma_p^{\max}$ is the maximum principal stress and X_T is the tensile strength of bulk adhesive.
Adhesive failure can also be due to bondline failure [11]. This mechanism is complicated because decohesion and debonding of the interface usually occur together. Moreover, the strength of the adhesive/adherents interface is difficult to measure. Several engineering failure criteria have been proposed to combine these two mechanisms. In reference [11], the authors retain the following criteria which have been used by Tong and Steven [14]:

$$\left(\frac{\sigma_{yy}}{F_{peel}}\right)^2 + \left(\frac{\tau_{xy}}{F_{shear}}\right)^2 + \left(\frac{\tau_{zy}}{F_{shear}}\right)^2 = 1 \tag{6}$$

$$\left(\frac{\tau_{xy}}{F_{shear}}\right)^2 + \left(\frac{\tau_{zy}}{F_{shear}}\right)^2 = 1 \tag{7}$$

where σ_{zz}, τ_{xz}, τ_{yz} are the peel and shear stresses in the adhesive and F_{peel} and F_{shear} are the bondline peel and shear strengths. When shear is dominant, peel stress can be neglected, and the failure criterion can be written as

$$\frac{\sqrt{\tau_{xy}^2 + \tau_{zy}^2}}{F_{shear}} = 1 \tag{8}$$

In the same way, when peel is dominant, shear stresses are excluded, and the failure criterion can be written as

$$\frac{\sigma_{yy}}{F_{peel}} = 1 \tag{9}$$

3.5 Application to the local model

A Matlab routine give results everywhere in the adhesive. Figure 12 shows displacement along the $y-axis$ for the critical load. These displacements are concordant with the global model. This method gives a smooth solution for displacement along the $y-axis$.

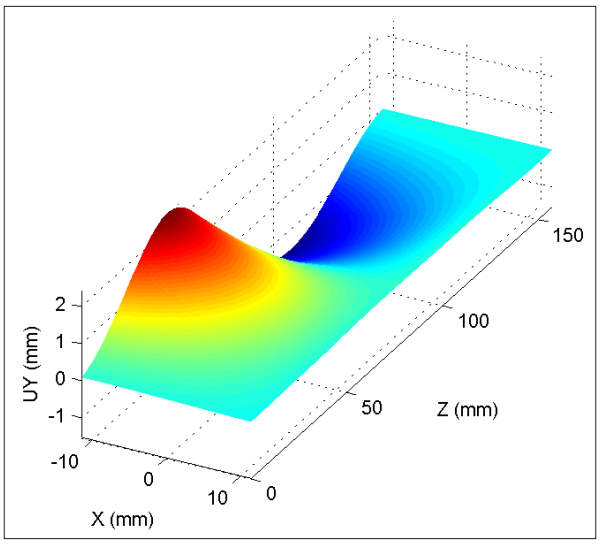

Fig. 12 Displacement in the adhesive along the $y-axis$ for the critical load

3.5.1 Maximum strain criterion

Elastic shear strain limit at room temperature γ_e is taken as equal to 0.0804 [15]. S_{eqv} is deduced by using equation 10, $S_{eqv} = 0.07$

$$\frac{\gamma_e}{2} = \frac{S_{eqv}}{\sqrt{3}} \tag{10}$$

Figure 13 shows $\varepsilon_{eqv}/S_{eqv}$ evaluated on each node inside the adhesive. The most stressed part, in line with this criterion, corresponds to the inflexion point shown in figure 12.

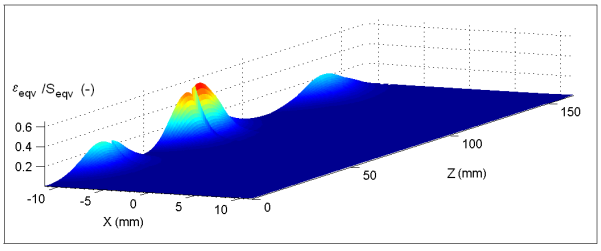

Fig. 13 $\varepsilon_{eqv}/S_{eqv}$ in the adhesive for the critical load

3.5.2 Maximum principal stress criterion

The tensile strength of the bulk adhesive is equal to 60.4 MPa [6]. This is in line with the figure 5. Ignition failure in the spew fillet will appear on the edge next to the web. Because of the joint

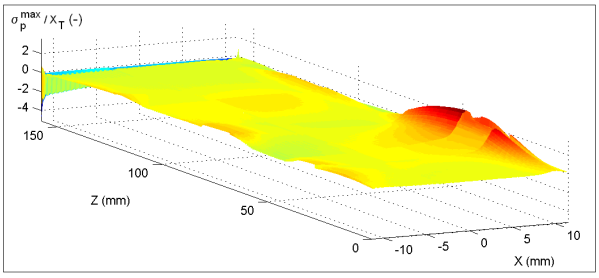

Fig. 14 σ_p^{max}/X_T in the adhesive for the critical load

configuration, singular stress/strain fields appear [11]. Adams Peppiatt states that sharp corners do not exist in real joints and therefore neither do stress/strain singularities [16]. It has been pointed out that reasonable results has been obtained with maximum stress failure criteria when an averaged value is used. Thus, a way to avoid singularities is to use the criterion at a given distance from the singularity point. This distance is called the characteristic distance [11].

3.5.3 Bondline failure criteria

Bondline peel and shear strength can be ascertained from the above criteria by using the failure stresses measured in tensile shear experiments [11]. The bondline shear strength given in Higgins' paper [17] is reproduced in table 1 and F_{peel} is considered as equal to 60.4 MPa. It gives the

F_{peel} (MPa)	F_{shear} (MPa)
60.4	37.2

Table 1 Bondline peel and shear strength at room temperature [17] [6]

results shown in figure 15. Edges and corners are more stressed than the rest of the adhesive.

Contrary to the displacement along the $y-axis$, there are more discontinuities in figures 13, 14 and 15. This is due to the assembly of the various local models. Performing another set of local models around relevant points would improve accuracy.

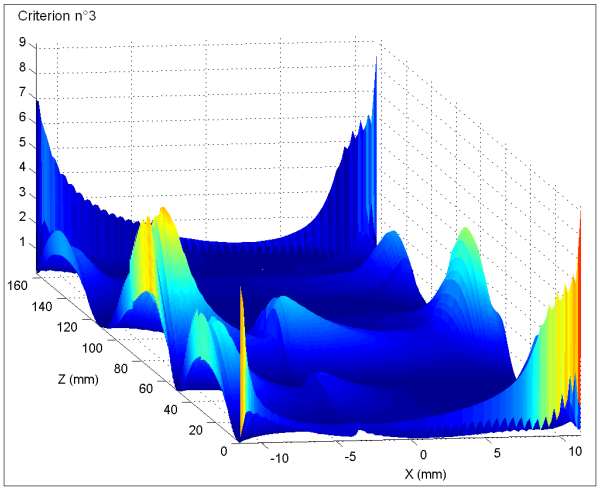

Fig. 15 Criterion $n°3$ in the adhesive at critical load

4 Conclusions

A global-local approach to analyse the behaviour of adhesive has been presented. It enables weak zones in the adhesive to be defined and checks, using criteria found in the literature, whether the bonded joint will resist until the critical load is reached. This method confirms that edges are more susceptible to failure due to stress concentration.

Even if the graph representing displacement along the $y-axis$ does not show any discontinuity because of the assembly of seven local models, each individual criterion presents some discontinuity. Therefore, for greater accuracy, it may be useful to recompute a local model around the critical area.

This first approach uses beam elements to model adhesive in the global model. Another way to tackle the problem is to employ nonlinear shear and normal springs between nodes to approximate the inherent flexibility of the bonded joints. Compared to simulations approximating the bonded joints with infinite rigidity, the drop in post-buckling performance is significant, of the order of $10-20\%$ depending on the type of buckling. Deformations in the post-buckled state are significantly greater. It is therefore of great importance to incorporate the flexibility of the adhesive into the global model.

References

[1] A. Murphy, M. Price, P. Wang. The integration of strength and process modeling of friction-stir-welded fuselage panels. *American Institute of Aeronautics and Astronautics*, AIAA 2005-2026:1–15, 2005.

[2] Jeff W.H. Yap, Murray L. Scott, Rodney S. Thomson, Dieter Hachenberg. The analysis of skin-to-stiffener debonding in composite aerospace structures. *Composite Structures*, 57:425–435, 2002.

[3] Sjoerd van der Veen, Adrian Murphy, Rinze Benedictus. Post-buckling failure of welded aluminium panels.

[4] Edward W. Thrall, Raymond W. Shannon. *Adhesive bonding of aluminum alloys*. Dekker, 1985.

[5] John Tomblin, Waruna Seneviratne, Paulo Escobar, Yap Yoon-Khian. Shear stress-strain data for structural adhesives. Technical Report DOT/FAA/AR-02/97, Office of Aviation Research, November 2002.

[6] Kwang-Soo Kim, Jae-Seok Yoo, Yeong-Moo Yi, Chun-Gon Kim. Failure mode and strength of uni-directional composite single lap bonded joints with different bonding methods. *Composite Structures*, 72:477–485, 2006.

[7] Eduard Riks, Charles C. Rankin, Francis A. Brogan. On the solution of mode jumping phenomena in thin-walled shell structures. *Computer Methods in Applied Mechanics and Engineering*, 136:59–92, 1996.

[8] Wilhelm Rust, Karl Schweizerhof. Finite element limit load analysis of thin-walled structures by ansys (implicit), ls-dyna (explicit) and in combination. *Thin-Walled Structures*, 41:227–244, 2003.

[9] *MSC.Marc Volume A: Theory and User Information*, 2005.

[10] *MSC.Marc Volume C: Program Input*.

[11] Phil Yarrington, James Zhang, Craig Collier, Brett A. Bednarcyk. Failure analysis of adhesively bonded composite joints. *American Institute of Aeronautics and Astronautics*, AIAA 2005-2376:1–23, 2005.

[12] R.B. Heslehurst, L. Hart-Smith. The science and art of structural adhesive bonding. *SAMPE*

Journal, 38:60–71, 2002.

[13] D. M. Hoyt, Stephen H. Ward, Pierre J. Minguet. Strength and fatigue life modeling of bonded joints in composite structure. *Journal of Composites Technology and Research*, 24, 2002.

[14] L. Tong, G.P. Steven. *Analysis and Design of Structural Bonded Joints*. Kluwer Academic Publishers, 1999.

[15] Peter Chalkley , John van den Berg. On obtaining design allowables for adhesives used in the bonded-composite repair of aircraft. Technical Report DSTO-TR-0608, Defence Science and Technology Organisation, January 1998.

[16] R.D. Adams, N.A. Peppiatt. Stress analysis of adhesive-bonded lap joints. *Journal of Strain Analysis*, 9:185–196, 1974.

[17] A. Higgins. Adhesive bonding of aircraft structures. *International Journal of Adhesion and Adhesives*, 20:367–376, 2000.